

Boundary time crystals

F. Iemini,¹ A. Russomanno,^{2,1} J. Keeling,³ M. Schirò,⁴ M. Dalmonte,¹ and R. Fazio^{1,2}

¹ICTP, Strada Costiera 11, 34151 Trieste, Italy

²NEST, Scuola Normale Superiore & Istituto Nanoscienze-CNR, I-56126, Pisa, Italy

³SUPA, School of Physics and Astronomy, University of St Andrews, St Andrews, KY16 9SS, United Kingdom

⁴Institut de Physique Théorique, Université Paris Saclay, CNRS, CEA, F-91191 Gif-sur-Yvette, France

(Dated: June 28, 2018)

In this work we introduce *boundary time-crystals*. Here *continuous* time-translation symmetry breaking occurs only in a macroscopic fraction of a many-body quantum system. After introducing their definition and properties, we analyse in detail a solvable model where an accurate scaling analysis can be performed. The existence of the boundary time crystals is intimately connected to the emergence of a time-periodic steady state in the thermodynamic limit of a many-body open quantum system. We also discuss connections to quantum synchronisation.

Introduction - Spontaneous symmetry breaking is a cornerstone of physics and occurs at all energy scales, in cosmology and high-energy physics as well as in condensed matter. Thermal or quantum fluctuations can drive a system into a state that breaks, in the thermodynamic limit, some of the symmetries present in its (thermo)-dynamical potentials [1, 2]. Can time-translation invariance be spontaneously broken? The possible existence of time crystals, first addressed by Wilczek in [3], prompted an intense discussion [4–7]. A no-go theorem [9] ruled out the existence of time-crystals in thermal equilibrium in cases for which the energy is the only constant of motion. The situation may be different in the presence of additional extended conserved quantities [10], such as in superfluids [11] where time-crystalline behavior was discussed in [12]. Ordering in time can also occur, however, under non-equilibrium conditions (e.g. by preparing the system in an excited state [13]).

An important step forward in our understanding of spontaneous time-translational invariance has been achieved in [8, 14, 15] where Floquet time crystals, a.k.a. π -spin glasses, were introduced. The dynamics of these systems, subject to a periodic driving, is characterised by observables which oscillate at a multiple of the driving period. Hence they break the *discrete* time-translation symmetry imposed by the external drive. Floquet time crystals were intensively explored from a theoretical point of view in [16–22] and very recently experimentally observed [23, 24]. A comprehensive review on time crystals can be found in [25].

Here we predict a novel form of time-translation symmetry breaking: *continuous Boundary Time-Crystals* (BTCs). In the BTC phase, symmetry breaking appears in a (macroscopic) fraction of the system. Moreover a BTC breaks the continuous time-translation symmetry, i.e. the system self-organises in a time-periodic pattern with a period which only depends on its coupling constants. The idea borrowed from surface critical phenomena [26] offer a very intuitive way to visualise BTCs. Only the surface, representing the portion of the system where time crystalline behaviour appear, is ordered. The rest

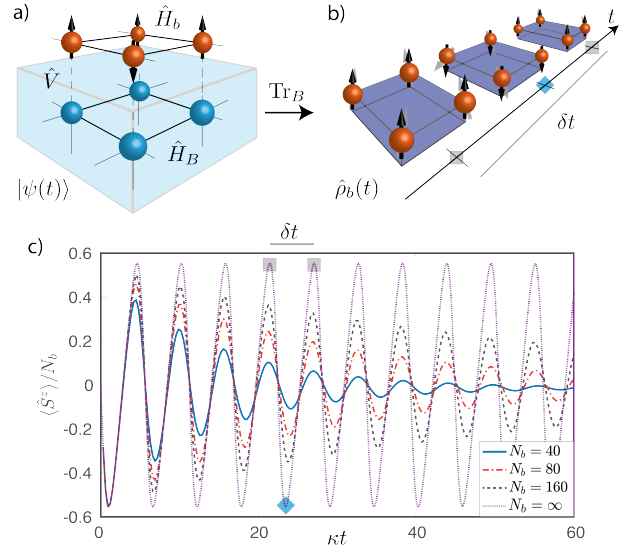


Figure 1. (Upper panel) A sketch of a boundary time crystal. The system is composed by a bulk (B) and a boundary (b) interacting through an interaction term \hat{V} . The Hamiltonian of the system is time-independent. After tracing out the degrees of freedom of the bulk, the dynamics of the boundary is described by the reduced density matrix $\hat{\rho}_b$. In the time-crystal phase, the behaviour of collective variables will show persistent oscillations in the thermodynamic limit. (Lower panel) The boundary magnetisation of the BTC model discussed in the paper is shown as a function of time, for different boundary sizes. In the asymptotic condition, spontaneous symmetry breaking appears in persistent oscillations when $N_b \rightarrow \infty$.

of the system, the bulk remains time-translationally invariant, see Fig. 1. We will give a more precise meaning to this picture in the following of the paper where we will show that BTCs are intimately connected to the existence of periodic motion in the steady state of open quantum many-body systems.

Boundary time crystals - The emergence of a BTC can be understood using the sketch given in Fig. 1 (top panels). A d -dimensional quantum many-body system is governed by a time-independent Hamiltonian $\hat{H} =$

$\hat{H}_B + \hat{H}_b + \hat{V}$, with bulk and boundary systems \hat{H}_B and \hat{H}_b , respectively, and an interaction term \hat{V} . Denoting as N_b (N_B) the degrees of freedom for the boundary (bulk) systems, we consider the case in which a macroscopic fraction of the universe, the system ($N_b \rightarrow \infty$), breaks spontaneously time-translational invariance. The thermodynamic limit is performed with $N_b, N_B \rightarrow \infty$, with the ratio $N_b/N_B \rightarrow 0$. In other words, it is a macroscopic system, but still small/infinitesimal compared to the global system. This scaling is the crucial feature in defining a boundary phenomenon. The precise identification of the boundary layer (*e.g.* the nature or any notion of spatial locality for its degrees of freedom) is thus irrelevant for our purposes. The whole system evolves according to the Schrödinger equation $|\psi(t)\rangle = e^{-i\hat{H}t}|\psi(0)\rangle$, with $|\psi(0)\rangle$ the initial state of the quantum system. The boundary is fully characterised by the reduced density matrix $\hat{\rho}_b = \text{Tr}_B(|\psi(t)\rangle\langle\psi(t)|)$ obtained by tracing out the bulk degrees of freedom. Its dynamics is governed by a completely positive, trace-preserving, map $\hat{\mathcal{L}}$ with

$$\frac{d}{dt}\hat{\rho}_b = \hat{\mathcal{L}}[\hat{\rho}_b]. \quad (1)$$

Time-translation symmetry breaking at the boundary appears as a non-trivial time-dependence of a (macroscopic) boundary order parameter \hat{O}_b , occurring only in the thermodynamic limit. For infinitely large times its expectation oscillates, $\lim_{N_b, N_B \rightarrow \infty} \text{Tr}[\hat{O}_b \hat{\rho}_b] = f(t)$ where $f(t)$ is a time-periodic function. The definition of BTC closely follows the one for the standard time crystals [9, 16, 17]. The only, crucial, difference is that here the order parameter is defined at the boundary.

The resulting physical picture is exemplified in Fig. 1, taking a magnetic system as an illustration. In this example a macroscopic magnetisation builds up at the surface of a sample. The magnetisation shows persistent oscillations even though the dynamics of the whole system is governed by a time-independent Hamiltonian. In Fig. 1 the boundary and the bulk are represented with different symbols in order to stress that they may be described by different degrees of freedom. Notice that the terms bulk and boundary are used here to easily visualise the mechanism of spontaneous symmetry breaking and suggest an intriguing connection with boundary critical phenomena. What is really implied in the construction above is that ordering in time occurs only in a macroscopic fraction of the many-body system under consideration, rather than in the whole bulk.

The boundary nature of time-translation symmetry breaking in BTC has a number of important implications. First of all, the reduced density matrix $\hat{\rho}_b$ in the steady state will be generically non-thermal, hence the no-go theorem [9] does not apply: a Hamiltonian system can spontaneously break time-translation symmetry as a boundary phase. Furthermore, given the well known correspondence of the dissipative dynamics in Eq.(1)

and a unitary dynamics governed by a time-independent Hamiltonian on an enlarged system (see *e.g.* [27]), the BTC appears tightly linked to the existence of a time-periodic steady state in an open quantum many-body system, appearing though *only* for $N_b \rightarrow \infty$. In order to discuss concrete examples we focus on boundary systems described by Markovian maps, and comment further below about more general dissipative maps.

The evolution of the boundary in the Markovian case is described by a master equation where the Liouvillian operator $\hat{\mathcal{L}}[\cdot]$ has Lindblad form [27], $\hat{\mathcal{L}}[\cdot] = \sum_{\alpha} \left\{ \hat{\ell}_{\alpha} \cdot \hat{\ell}_{\alpha}^{\dagger} - \frac{1}{2} \{ \hat{\ell}_{\alpha}^{\dagger} \hat{\ell}_{\alpha}, \cdot \} \right\}$ with $\hat{\ell}_{\alpha}$ the Lindblad operators [28]. The emergence of a time-crystal behaviour in the long-time dynamics of the system is hidden in the properties of the Liouvillian operator in the thermodynamic limit. In the BTC phase one should expect: i) a vanishing gap in the real part of the Liouvillian eigenvalues, making the non-equilibrium steady state subspace degenerate in the thermodynamic limit with time-dependent coherences decaying over an infinite time-scale; ii) a non-zero imaginary part for some Liouvillian eigenvalues in such subspace in order to induce non-trivial oscillations. The main question now is to find a many-body system that displays the above mentioned properties. Below we will present a model of a BTC.

A BTC model - We will show that a boundary time crystal appears in a model used to describe cooperative emission in cavities (see [3–6, 29, 32]). The boundary Hamiltonian $\hat{H}_b = \omega_0 \sum_j \hat{\sigma}_j^x$ consists in a collection of 1/2-spins whose dynamics is governed by collective spin operators $\hat{S}^{\alpha} = \frac{1}{2} \sum_j \hat{\sigma}_j^{\alpha}$. The operators $\hat{\sigma}_j^{\alpha}$ ($\alpha = x, y, z$) are the Pauli matrices acting on the j -th spins, and ω_0 is the coherent splitting. The terms \hat{H}_B and \hat{V} (see the sketch in Fig. 1) have to be constructed in such a way to give a reduced dynamics at the boundary of the form

$$\frac{d}{dt}\hat{\rho}_b = i\omega_0[\hat{\rho}_b, \hat{S}^x] + \frac{\kappa}{S} \left(\hat{S}_- \hat{\rho}_b \hat{S}_+ - \frac{1}{2} \{ \hat{S}_+ \hat{S}_-, \hat{\rho}_b \} \right). \quad (2)$$

In the previous equation, the collective raising/lowering spin operators are given by $\hat{S}_{\pm} = \hat{S}^x \pm i\hat{S}^y$, κ is the effective decay rate, and $S = N_b/2$ is the total spin. In the following the expectations of the observables are indicated as $\langle \cdot \rangle = \text{Tr}[\cdot \hat{\rho}_b]$.

The specific form of \hat{H}_B generating the dynamics in Eq. (2) will play no role. It is possible to derive it [28]. In the Supplementary Material we discuss in details how such a construction can be made [35]. Moreover similar Liouvillian dynamics have been extensively considered in the context of atomic systems coupled to cavity modes. Typically, the scenario in which a model such as Eq. (2) arises involves a system periodically driven at a finite frequency, with a time dependent Hamiltonian. Depending on the specific driving, such an explicit time dependence can be usually gauged away: one can define a Hamiltonian leading to Eq. (2) which is time-

independent in some specific choice of frame. As long as such a Hamiltonian exists, and is physical, our interpretation of the time-translation symmetry breaking as a boundary phenomenon of a closed quantum system is reasonable (see [35] for a detailed discussion). Moreover – as we are going to show – the BTC shows a time-dependent pattern whose period solely depends on the coupling constants of the system and which is in general incommensurate with the driving period: the system breaks a continuous symmetry, rather than a discrete one. The BTC is in apparent contradiction with the expectation that the density matrix of a system in contact with a single thermal reservoir attains a time-independent steady state [36]. The solution to this apparent paradox lies in the diverging boundary size, $N_b \rightarrow \infty$, which leads to a divergent decay time-scale for oscillations (see [35]), as we better discuss below.

The steady state diagram of the model has two distinct phases [29]. For $\omega_0/\kappa < 1$, the total magnetisation is finite $\langle S^z \rangle$. In the opposite case, $\omega_0/\kappa > 1$, all spins align along the x -direction. More details are reported in [35].

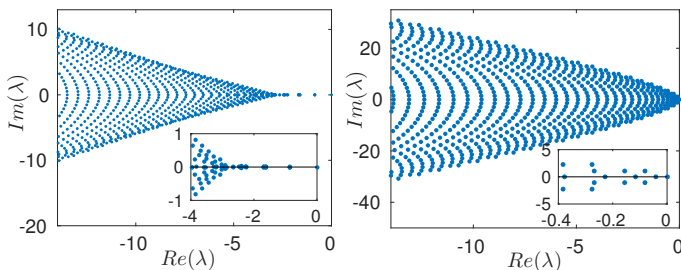


Figure 2. The eigenvalues λ of the Liouvillian are shown in the weak dissipative case ($\omega_0/\kappa = 1.5$ – right panel) and in the strong dissipative one for ($\omega_0/\kappa = 0.5$ – left panel), in a system with $N_b = 36$ spins. The insets show a zoom over the eigenvalues with largest real part. The eigenvalues are plotted in units of κ .

The BTC appears for $\omega_0/\kappa > 1$. Its emergence is embedded in the properties of the eigenvalues λ of the Liouvillian $\hat{\mathcal{L}}$. The structure of the Liouvillian spectrum is indeed different in the two phases. While for $\omega_0/\kappa < 1$ the spectrum is gapped (Fig. 2 left panel), and the eigenvalues with greatest values for their real part (*i.e.*, the eigenvalues closest to zero, recalling that $Re(\lambda_j) \leq 0$) have no imaginary values, for $\omega_0/\kappa > 1$ the spectrum becomes gapless and the eigenvalues with greatest real part have a non zero imaginary part (see Fig. 2). The insets zoom on the spectrum emphasising the different behaviour in the two limits.

In order to obtain a quantitative picture of the development of the spontaneous symmetry breaking we perform a finite-size scaling analysis of the real and imaginary parts of the eigenvalues λ . In Fig. 3 (left panel) we analyse the real part of the Liouvillian spectrum. In the weak

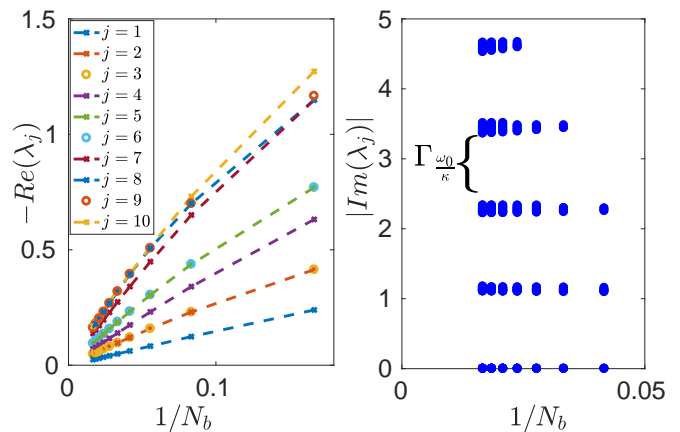


Figure 3. (Left) Finite size scaling for the real part of the Liouvillian eigenvalues in the BTC phase. The index j labels the eigenvalues. The Liouvillian eigenvalues λ_j are ordered as a function of their real part ($|Re(\lambda_j)| \leq |Re(\lambda_{j+1})|$, and $j = 0$ has zero real part). In the $\omega_0/\kappa > 1$ phase they scale to zero as a power-law of the inverse system size. (Right) The imaginary parts of the eigenvalues show a band structure, with a fundamental frequency separation $\Gamma_{\omega_0/\kappa}$. For fixed excitation thresholds (we only select λ_j such that $\nu = j^2/N_b \leq \epsilon$) the width of the bands remains finite in the thermodynamic limit (here we choose $\nu < 0.025$). The widths of the bands tend to decrease as we constrain to lower excitation thresholds. The eigenvalues are plotted in units of κ .

dissipative case, the one of interest to us, the system is gapless, with the real part of the eigenvalues closing with the system size as a power law (at different rates). In Fig. 3 (right panel) we show the imaginary part of the Liouvillian spectrum. The imaginary eigenvalues of the low Liouvillian excitations are described by bands, separated by a fundamental frequency $\Gamma_{\omega_0/\kappa}$, which depends on the system parameters ω_0/κ . These features of the real and imaginary parts are the key elements for the appearance of the BTC.

The magnetisation, for different numbers of lattice sites, is plotted in Fig. 1 (lower panel). The system is initialised in the pure state with all spins aligned along the x -direction. The oscillations decay for any finite size system, the associated time scale grows with the system size and diverges in the thermodynamic limit. This behaviour is independent of the initial conditions, as *e.g.*, starting from thermal states or all spins aligned in different directions. Interestingly, the decay rate of the oscillations η is related to the second excited eigenvalue of the Liouvillian, in our case, the lowest excited eigenvalue with non zero imaginary value (eigenvalues are ordered according to the absolute value of their real part). A quantitative analysis of the spontaneous symmetry breaking is obtained by looking at the Fourier transform of $\langle S^z(t) \rangle$ (see Fig. 4). By performing a spectral analysis, we see that the peaks appear at frequencies related to the separation between the bands shown in the right panel of

Fig. 3. The peaks become sharper as the system size is increased. Most importantly, the decay rate η goes to zero (right panel) as a power law $L^{-\beta}$ with the β exponent dependent on the system parameters w_0/κ . The finite-size scaling shows that the persistent oscillations are associated to the spontaneous time-translation symmetry breaking because they occur *only* in the thermodynamic limit. In the example we have discussed, the thermodynamic limit incidentally coincides with an effective classical dynamics (the effective Planck's constant going to zero): this is true for instance in Fig. 4 and in Fig. 1 when $N_b \rightarrow \infty$; details of the classical solution are discussed in [35, 37].

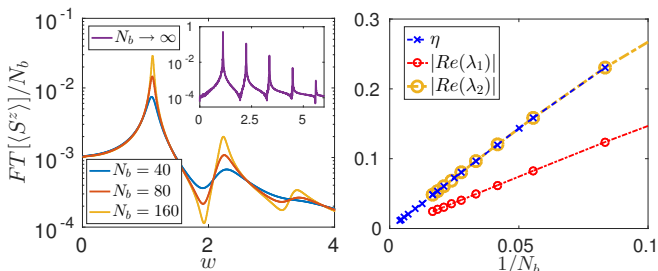


Figure 4. In the right panel we plot the decay rate of the oscillations of the magnetisation η for distinct system sizes. In the same plot we compare η with the eigenvalues with greatest real part - thus smallest absolute values for the real part of the Liouvillian. In the left panel we plot the Fourier transform of the average magnetisation (see lower panel in Fig. 1), highlighting the oscillation frequencies of the dynamics. The peaks are associated to the band separations in the imaginary part discussed in Fig. 3. The inset of the left panel is the solution in the thermodynamic limit where the oscillations persist indefinitely.

From the experimental point of view, a driven version of this model can be realised using an adapted Raman driving scheme [38] for cold atoms in an optical cavity, connecting two low lying states via an excited atomic state. Collective dissipation can be produced by using a bad cavity (large loss rate) combined with a single Raman drive: Purcell-enhanced Raman scattering leads to optical pumping of the atoms, described by the same collective dissipation considered here. Similarly, the Hamiltonian term \hat{S}^x can be realised by a pair of drive lasers coupling the ground states via excited states.

The boundary time-crystal we discussed in the model of Eq.(2) is not an isolated point, but is robust to different perturbations. First of all, the time-crystalline phase appears in the whole region $\omega_0/\kappa > 1$. Moreover it is stable if additional perturbations are added to the unitary part of the evolution. With a boundary Hamiltonian of the form $\hat{H}_b = \omega_0 \hat{S}^x + \omega_x (\hat{S}^x)^2/S + \omega_z (\hat{S}^z)^2/S$, the time-crystal is still present for a wide range of the parameters $\omega_x, \omega_z \neq 0$. In fact the ω_x term improves the stability of the time crystal, which is also present for small values of ω_z ; for ω_z above some threshold, time-translation

symmetry breaking still exists but only for some initial conditions (see [35] for details). It is worth mentioning that robustness of a BTC phase refers to the persistence of a periodic evolution in the thermodynamic limit, and not necessarily to the rigidity of its period. The main difference with respect to Floquet systems is that there, since one is breaking a discrete symmetry, rigidity is intimately related to the period of the driving; instead, in our case, since the dynamics is $U(1)$ invariant, such timescale is not present, and the period of oscillation is allowed to change within the symmetry-broken phase. This is a direct analog of the fact that in spatial crystals, the spatial periodicity can be changed by changing the particle-particle interaction.

It is also relevant to consider perturbations of the dissipative part of the evolution, more specifically we focus on terms non-local in time (this is equivalent to considering a non-Markovian equation of motion). In order to have a physical bulk Hamiltonian, it must be bounded from below, and so it cannot have a truly flat density of states. This implies a finite memory timescale for the bath, but there is the possibility that this timescale can be neglected, being far smaller than all the other timescales in the system dynamics. This fact occurs if the lower bound on the bulk spectrum is at energies much lower than the frequencies of the system dynamics: in this case an approximate Markovian description holds and the use of a Markovian master equation is perfectly justified.

Other candidate systems for BTCs - An interesting model that should show the same phenomenology has been studied in [39]. Furthermore, many-body limit cycles have been already seen in model systems of optomechanical arrays [40], coupled cavity arrays [41, 42], interacting Rydberg atoms [43] and interacting spin-systems [44]. Also in these cases the underlying (bulk+boundary) Hamiltonian can be constructed, see Ref. [35]. In light of the analysis performed in the present work, these limit-cycles now might be classified as BTCs. It should be however kept in mind that a mean-field approximation, employed in these works, may be unable to support the very existence of limit cycles: it is not clear to which extent this phase would survive when fluctuations are included.

Other promising systems that it might be interesting to consider to seek for different forms of BTCs are dissipative topological systems. In this case the steady state may develop a degeneracy in the thermodynamic limit due to the presence of edge states [45, 46]. The existence of a BTC phase should emerge from the competition of the unitary and dissipative parts of the dynamics. Furthermore the robustness should be inherently linked to topological protection.

Finally a BTC, corresponding to a space-time ordering, represents in essence a synchronised dynamics in a many-body open quantum system. This hints to a very interesting and deep connection between time crystals

and quantum synchronisation. Lately there has been an intense effort to characterise synchronisation in the quantum realm (see e.g., the review [47]). BTCs may offer a different perspective on this problem.

Conclusions - In this work we introduced boundary time crystals. In the same spirit as in the original definition given in [9], in the BTC phase the time-dependent order parameter appears only in a portion of the sample (at the boundary for simplicity). The phenomenon is analogous to surface critical phenomena. On looking at the reduced dynamics at the boundary, one observes that BTCs are intimately linked to the emergence of a periodic dynamics in some macroscopic observable of an open quantum many-body system. A crucial aspect of the whole picture is that the periodic motion should appear *only* in the thermodynamic limit. We proposed an example of a BTC phase in a solvable model where its existence can be confirmed without resorting to any approximation. We finally discussed that BTCs can also emerge from different mechanisms in topological systems.

While completing this manuscript, a few works appeared [48, 49] analysing *discrete* time crystal phenomena in periodically driven dissipative systems.

Acknowledgements - We acknowledge enlightening discussions with S. Denisov, J. Jin, L. Mazza, T. Prosen, and P. Zoller. This work was supported in part by “Progetti Interni - Scuola Normale Superiore” (A.R.), EU-691 QUIC (R.F. and A.R.), CRF Singapore Ministry of Education (CPR-QSYNC 692) (R.F.), EPSRC program TOPNES (EP/I031014/1) (J.K.),

-
- [1] N. Goldenfeld, *Lectures on phase transitions and the renormalization group*, (Addison Wesley, New York, 1992).
- [2] S. Sachdev, *Quantum Phase Transitions*, (Cambridge University Press, Cambridge, 2000).
- [3] F. Wilczek, Phys. Rev. Lett. **109**, 160401 (2012).
- [4] T. Li, Z.-X. Gong, Z.-Q. Yin, H. T. Quan, X. Yin, P. Zhang, L.-M. Duan, and X. Zhang, Phys. Rev. Lett. **109**, 163001 (2012).
- [5] P. Bruno, Phys. Rev. Lett. **110**, 118901 (2013); *ibid* **111**, 029301 (2013); *ibid* **111**, 070402 (2013).
- [6] P. Nozieres, EPL **103**, 57008 (2013).
- [7] G. E. Volovik, JETP Lett. **98**, 491 (2013).
- [8] K. Sacha, Phys. Rev. A **91**, 033617 (2015).
- [9] H. Watanabe and M. Oshikawa, Phys. Rev. Lett. **114**, 251603 (2015).
- [10] D. Huse (private communication).
- [11] Hadrien Kurkjian, Yvan Castin and Alice Sinatra, Comptes Rendus Physique **17**, 789 (2016).
- [12] Nikolay V. Prokof'ev and Boris V. Svistunov, arXiv:1710.00721.
- [13] A. Syrwid, J. Zakrzewski, and K. Sacha, Phys. Rev. Lett. **119**, 250602 (2017).
- [14] D. V. Else, B. Bauer, and C. Nayak, Phys. Rev. Lett., **117**, 090402 (2016).
- [15] V. Khemani, A. Lazarides, R. Moessner, and S. L. Sondhi, Phys. Rev. Lett. **116**, 250401 (2016).
- [16] C. W. von Keyserlingk, V. Khemani, and S. L. Sondhi, Phys. Rev. B **94**, 085112 (2016).
- [17] V. Khemani, C. W. von Keyserlingk, S. L. Sondhi, arXiv:1612.08758.
- [18] D. V. Else, B. Bauer, and C. Nayak, Phys. Rev. X **7**, 011026 (2017).
- [19] N.Y. Yao, A.C. Potter, I.-D. Potirniche, and A. Vishwanath, Phys. Rev. Lett. **118**, 030401 (2017).
- [20] W. W. Ho, S. Choi, M. D. Lukin, and D.A. Abanin, Phys. Rev. Lett. **119**, 010602 (2017).
- [21] B. Huang, Y.-H. Wu, W.V. Liu, arXiv:1703.04663.
- [22] A. Russomanno, F. Iemini, M. Dalmonte, and R. Fazio, Phys. Rev. B **95**, 214307 (2017).
- [23] J. Zhang, P. W. Hess, A. Kyprianidis, P. Becker, A. Lee, J. Smith, G. Pagano, I. D. Potirniche, A. C. Potter, A. Vishwanath, N. Y. Yao, and C. Monroe, Nature **543**, 217 (2017).
- [24] S. Choi, J. Choi, R. Landig, G. Kucsko, H. Zhou, J. Isoya, F. Jelezko, S. Onoda, H. Sumiya, V. Khemani, C. von Keyserlingk, N. Y. Yao, E. Demler, and M. D. Lukin, Nature **543**, 221 (2017).
- [25] K. Sacha and Jakub Zakrzewski, arXiv:1704.03735.
- [26] K. Binder, in Phase transitions and critical phenomena, Vol. 8 pag 2, C. Domb and J.L. Lebowitz Eds (Academic Press, New York, 1983).
- [27] M. Nielsen and I. Chuang, *Quantum Computation and Quantum Communication*, (Cambridge University Press, Cambridge, 2000).
- [28] It is always possible to find a Hamiltonian whose dynamics is described by the given Lindblad equation. See e.g. Refs.[8, 50–54].
- [29] J. Hannukainen and J. Larson, arXiv:1703.10238.
- [30] D. F. Walls, P. D. Drummond, S. S. Hassan, and H. J. Carmichael, Prog. Theo. Phys. **64**, 307 (1978).
- [31] P. D. Drummond and H. J. Carmichael, Opt. Commun. **27**, 160 (1978).
- [32] R. R. Puri. and S. V. Lawande, Phys. Lett. A **72**, 200 (1979).
- [33] D. F. Walls, J. Phys. B: Atom. Molec. Phys. **13**, 2001-2009 (1980).
- [34] S. Schneider and G. J. Milburn, Phys. Rev. A **65**, 042107 (2002).
- [35] Supplementary Material
- [36] J. Cresser, J. Mod. Opt. **39**, 2187 (1992)
- [37] It is worth noticing that the peculiar classical dynamics studied in this article belongs to the class of reversible systems [11].
- [38] F. Dimer, B. Estienne, A. S. Parkins, and H. J. Carmichael, Phys. Rev. A **75**, 013804 (2007)
- [39] M. Hartmann, D. Poletti, M. Ivanchenko, S. Denisov, and P. Hänggi, New J. Phys. **19**, 083011 (2017).
- [40] M. Ludwig and F. Marquardt, Phys. Rev. Lett. **111**, 073603 420 (2013).
- [41] J. Jin, D. Rossini, R. Fazio, M. Leib, and M. J. Hartmann, Phys. Rev. Lett. **110**, 163605 (2013).
- [42] M. Schiró, C. Joshi, M. Bordyuh, R. Fazio, J. Keeling, and H. E. Türeci, Phys. Rev. Lett. **116**, 143603 (2016).
- [43] T. E. Lee, H. Häffner, and M. C. Cross, Phys. Rev. A **84**, 416, 031402 (2011).
- [44] C.-K. Chan, T. E. Lee, and S. Gopalakrishnan, Phys. Rev. A **91**, 051601 (2015).
- [45] S. Diehl, E. Rico, M. A. Baranov, and P. Zoller, Nat.

- Phys. **7**, 971 (2011).
- [46] F. Iemini, D. Rossini, R. Fazio, S. Diehl and L. Mazza, Phys. Rev. B **93**, 115113 (2016).
 - [47] F. Galve, G. L. Giorgi, and R. Zambrini, arXiv:1610.05060.
 - [48] Z. Gong, R. Hamazaki and M. Ueda, arXiv:1708.01472 (2017).
 - [49] R. R. W. Wang, B. Xing, G. G. Carlo and D. Poletti, arXiv:1708.09070 (2017).
 - [50] A. M. Chebotarev, Math. Notes, **61**, 510 (1997).
 - [51] M. Gregoratti, Commun. Math. Phys. **22**, 181 (2001).
 - [52] J. Gough, Open Systems & Information Dynamics, **22**, 1550009 (2015).
 - [53] Javier Prior, Alex W. Chin, Susana F. Huelga and Martin B. Plenio, Phys. Rev. Lett. **105**, 050404 (2010);
 - [54] Robert Rosenbach, Javier Cerrillo, Susana F. Huelga, Jianshu Cao and Martin B. Plenio, New. J. Phys. **18**, 023035 (2016).
 - [55] H. A. Sambe, Phys. Rev. A **7**, 2203 (1973).
 - [56] J.A.G.Roberts and G. R. W. Quispel, **216**, 63-177 (1992).

Supplementary Information for Boundary time crystals

F. Iemini, A. Russomanno, J. Keeling, M. Schirò, M. Dalmonte and R. Fazio

In this Supplementary Information we give more details on the model considered in Eq. (2) of the main text, the structure of its Liouvillian spectrum, and provide a full discussion of the classical effective model for $N_b \rightarrow \infty$. We also analyse the stability of the boundary time crystal when a perturbation of the type $(\hat{S}^z)^2$ is added to the Hamiltonian. For reader's convenience, we rewrite here the Lindblad equation

$$\frac{d}{dt}\hat{\rho} = i[\hat{\rho}, \hat{H}_b] + \frac{\kappa}{S} \left(\hat{S}_- \hat{\rho} \hat{S}_+ - \frac{1}{2} \{ \hat{S}_+ \hat{S}_-, \hat{\rho} \} \right), \quad (S1)$$

where

$$\hat{H}_b = \omega_0 \hat{S}^x + \frac{\omega_x}{S} (\hat{S}^x)^2 + \frac{\omega_z}{S} (\hat{S}^z)^2 \quad (S2)$$

and $N_b = 2S$. All the results in the main text are for $\omega_x = \omega_z = 0$. In the further sections we will show how they are extended to the more general case.

FROM HAMILTONIAN DYNAMICS TO THE MASTER EQUATION

In this section we add more details on the connection of Eq. (2) of the main text with an Hamiltonian dynamics and discuss how to apply a ‘‘chain-mapping’’ [1, 2] unitary transformation on the bath such that the bath have only local interactions and the system sits on its boundary. In this framework, we will also construct more general forms of boundary-bulk systems with the corresponding Hamiltonians.

We first compare two model Hamiltonians which lead to Eq. (2) in appropriate limits. A time-dependent Hamiltonian leading to driven oscillations, typically appearing in problems of atoms collectively coupled to a cavity [3–7], might take the form

$$\hat{H}_b = \omega_0 \hat{S}^z + \hat{S}^x \cos(\omega_0 t), \quad \hat{V} = \hat{S}^x (\hat{B} + \hat{B}^\dagger), \quad (S3)$$

where \hat{B} is a combination of bath operators. For this Hamiltonian, the existence of a large drive frequency ω_0 is necessary in order justify the approximation of neglecting fast oscillating terms in the system-bath Hamiltonian. However, Eq. (2) can also arise from a model in which counter-rotating terms are absent by definition (see for instance [5]),

$$\hat{H}_b = \omega_0 \hat{S}^z + \left(\hat{S}^+ e^{-i\omega_0 t} + \text{H.c.} \right), \quad \hat{V} = \hat{S}^+ \hat{B} + \text{H.c.} \quad (S4)$$

While such a model is not typically encountered, it remains physical (Hermitian, and bounded from below), and there exists a frame in which the time dependence vanishes. Even when considering this time-dependent Hamiltonian, we may note that the boundary time crystal corresponds to inducing a time dependence that is incommensurate with the driving term, hence the breaking of a continuous, rather than discrete symmetry.

We remark that the scenario we considered concerns an optical frequency drive, for which a rotating wave approximation (RWA) is valid. In this approximation one can perform a unitary transformation to a frame in which the Hamiltonian is time independent. At lower frequencies the RWA cannot be made and there is no frame in which the Hamiltonian is time independent. In these cases one can only define Floquet eigenvalues up to an integer multiple of the drive frequency [8], and the Floquet spectrum is periodic in energy. In contrast, when there exists a frame for which the Hamiltonian is time independent, it is possible to define eigenvalues in the ‘‘standard’’ way. The difference between these two cases can directly be traced to the presence or absence of counter-rotating terms in the effective Hamiltonian.

The physicality condition required can now be stated in a clearer way, in order to encompass cases where the RWA is possible and cases where Floquet theory must be applied: the bath spectrum should be bounded from below. We state this condition in order to exclude unphysical models where there is a continuous flow of energy into the bath

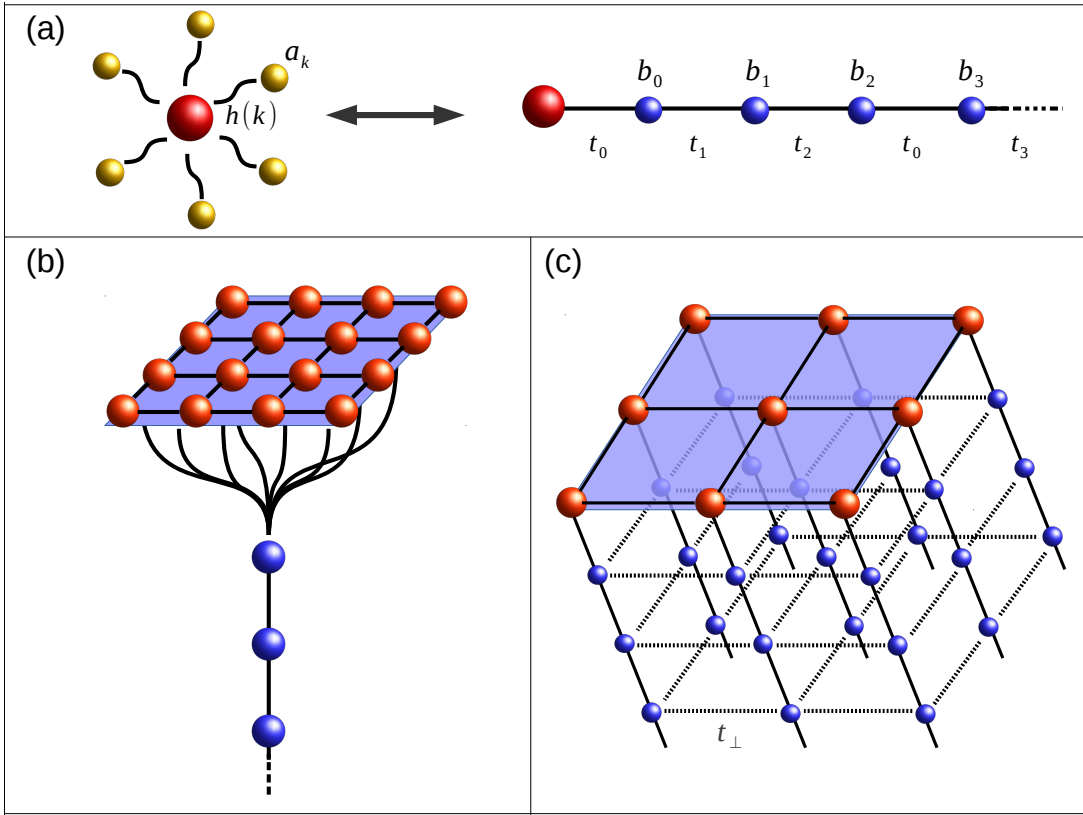


Figure S1. (a) A sketch on the chain mapping transformation, in which a general Hamiltonian system interacting with an environment composed of independent harmonic oscillators, as represented by the “star-shaped” picture, is mapped to a one-dimensional chain with only local and nearest-neighbor interactions. (b-c) Two distinct boundary systems from the perspective of the chain mapping transformation: in (b) the boundary system interacts collectively with the environment, while in (c) we consider the case in which all of the boundary elements interact with its own independent environment, thus leading to a lattice structure with $t_\perp = 0$. Small interactions $t_\perp \sim 0$ between nearby environmental modes shall not significantly influence the boundary system dynamics, and we may even consider a full (2 + 1)-dimensional lattice structure in these cases.

only because of its unbounded energy spectrum. A bath spectrum bounded from below leads to non-Markovian effects at very-short time scales that do not affect the existence of the time crystal.

Chain mapping: In a more general form, one can define a boundary system and its corresponding Hamiltonian by using the chain mapping transformation, precisely, an analytic transformation in which a general system interacting with an environment composed of harmonic oscillators is mapped to a one-dimensional chain with only local and nearest-neighbor interactions [1, 2]. The system after the transformation is described as a boundary of the chain. The details of such transformation are given as follows.

Consider a general system linearly interacting with an environment composed by independent harmonic oscillators. The total Hamiltonian can be described by,

$$\hat{H} = \hat{H}_S + \hat{H}_E + \hat{H}_{SE} \quad (S5)$$

where \hat{H}_S describes the system Hamiltonian, \hat{H}_E the environment, and \hat{H}_{SE} the system-environment interaction. Specifically,

$$\hat{H}_E = \int_0^{k_{\max}} g(k) a_k^\dagger \hat{a}_k dk \quad (S6)$$

$$\hat{H}_{SE} = \hat{A}_S \int_0^{k_{\max}} h(k) (a_k^\dagger + \hat{a}_k) dk \quad (S7)$$

where $a_k^\dagger (\hat{a}_k)$ are bosonic creation (annihilation) operators for the environmental modes, $g(k)$ its dispersion relation, k_{\max} denotes the cut-off for the spectral density, and the interaction is described by a general system operator \hat{A}_S coupled to environment displacement operators with strength $h(k)$.

Employing a bosonic basis transformation, one can map such “star-shaped” Hamiltonian to a one-dimensional chain with only local and nearest-neighbor interactions (see Fig.(S1)-(a)). The system is mapped to a boundary of the chain. This transformation is accomplished by representing the bath with the new following set of bosonic operators:

$$\hat{b}_n^\dagger = \int_0^{k_{\max}} U_n(k) a_k^\dagger dk \quad (\text{S8})$$

where U_n are the coefficients of a unitary transformation based on orthogonal polynomials [1]. The Hamiltonian in this new basis is described by $\tilde{H} = \tilde{H}_S + \tilde{H}_E + \tilde{H}_{SE}$, with

$$\tilde{H}_{SE} = t_0 \hat{A}_S \left(\hat{b}_0^\dagger + \hat{b}_0 \right), \quad (\text{S9})$$

$$\tilde{H}_E = \sum_{n=0}^{\infty} w_n \hat{b}_n^\dagger \hat{b}_n + t_n \left(\hat{b}_n^\dagger \hat{b}_{n+1} + h.c. \right), \quad (\text{S10})$$

where the effective hopping parameters t_n are determined by the bath dispersion relation.

The physical picture of a boundary system as defined in the main text then follows very naturally under such a chain-mapping transformation: in the limit $N_B \rightarrow \infty$, $N_b \rightarrow \infty$, $N_b/N_B \rightarrow 0$ (N_b and N_B are the system and environment degrees of freedom, respectively) the bath behaves as an infinite chain with the system always sitting on the boundary of this chain.

In Fig.(S1)-(b-c) we schematically illustrate two distinct boundary systems under the perspective of the chain-mapping transformation: (i) in the first case, as shown in Fig.(S1)-(b), we consider all spins of the boundary system collectively interacting with a single bosonic mode of the transformed basis (the model studied in this article corresponds to this class, with a collective coupling $\hat{A}_S \equiv \hat{S}_x$ – see Eq. (S3)); (ii) in a different setting, we can consider the case where each spin of the boundary system interacts independently with its own environment. In the latter case, by applying the chain-mapping transformation to each spin, we get the lattice structure of Fig.(S1)-(c). In both cases, under appropriate limits, such as weak coupling “ t_0 ” between system and environment, we can neglect memory effects on the system dynamics, in the limit of an infinite chain. The dynamics of the system under these limits can be approximated by a Markovian dynamics, as discussed in detail at the beginning of this section for the specific model studied in this article.

It is worth mentioning that the model considered in this article is particularly well suited for the study of BTC (boundary time crystal) due to the possibility of performing the scaling analysis (see Fig.2-4 in the main text). Time crystals are collective phenomena occurring only in the thermodynamic limit and it is extremely important to perform a scaling analysis in order to understand if this is the case. However, there are no arguments precluding the possibility of BTC’s in distinct systems, such as the lattice structure depicted in Fig.(S1)-(c). In fact, these models support limit cycles [9, 10] at the mean-field level. In these cases however the problem is currently intractable and one is not able to derive an exact solution. More specifically, the models in [9, 10] are realised by having an XYZ-Heisenberg or quantum-Ising Hamiltonian at the boundaries (red sites in the figure) and local baths ($t_\perp = 0$). The results are not expected to change qualitatively at small t_\perp .

PHASE DIAGRAM AND LIOUVILLIAN SPECTRUM

In all this section we assume $\omega_x = \omega_z = 0$. The phase diagram of the model is relatively simple, with just two distinct phases according to the ratio ω_0/κ : (i) if the dissipative part is the leading term ($\omega_0/\kappa < 1$ – strong dissipative phase) all spins are aligned along the z -direction, and the total magnetization is finite $\langle \hat{S}^z \rangle < 0$; (ii) on the other hand, if the driving Hamiltonian is the leading term ($\omega_0/\kappa > 1$ – weak dissipative phase) the expectation values of all spins tend to be aligned along the x -direction and now $\langle \hat{S}^z \rangle = 0$. In Fig. S2 we plot the expectation values of the collective spin operators (left panel) and their variances (right panel), highlighting the two distinct phases of the model.

As we show in the main text, the properties of the Liouvillian spectrum are crucial for the time-crystal behaviour. In particular, in the weak dissipative phase, the gap in the real part of the Liouvillian spectrum vanishes in the thermodynamic limit, giving rise to the persistent time-translation symmetry breaking oscillations. In Fig. S3, we show the finite size scaling for the real part of the Liouvillian eigenvalues in the two phases of the model. The Liouvillian eigenvalues λ_j are ordered in terms of their real part: $|Re(\lambda_j)| \leq |Re(\lambda_{j+1})|$. In the upper panel the system is in the phase $\omega_0/\kappa < 1$, and we clearly see a finite Liouvillian gap in the thermodynamic limit: no time-translation symmetry breaking occurs. On the opposite, in the lower panel the system is in the phase $\omega_0/\kappa > 1$, and we see that the real part of the eigenvalues vanishes polynomially in N_b .

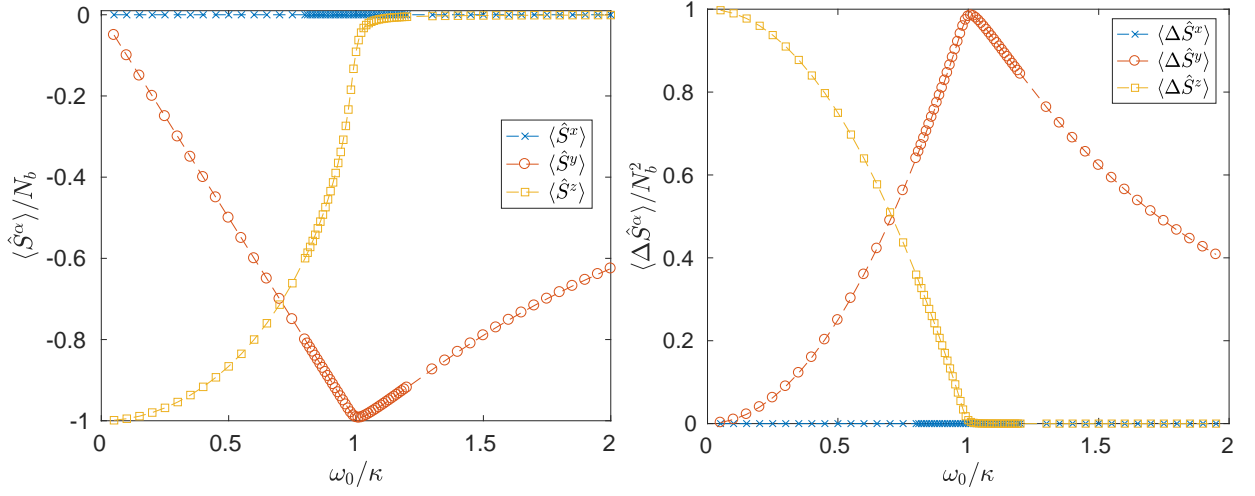


Figure S2. Expectation value for distinct observables for the non equilibrium steady state (NESS) of the Liouvillian in Eq. (2) - this state is unique for finite systems - in a system with $N_b = 600$ spins. On the *left panel* we plot the expectation value for the collective spins, as a function of the ratio ω_0/κ , and on the *right panel* the expectation value of their variances. In both panels we have fixed $\omega_z = 0$.

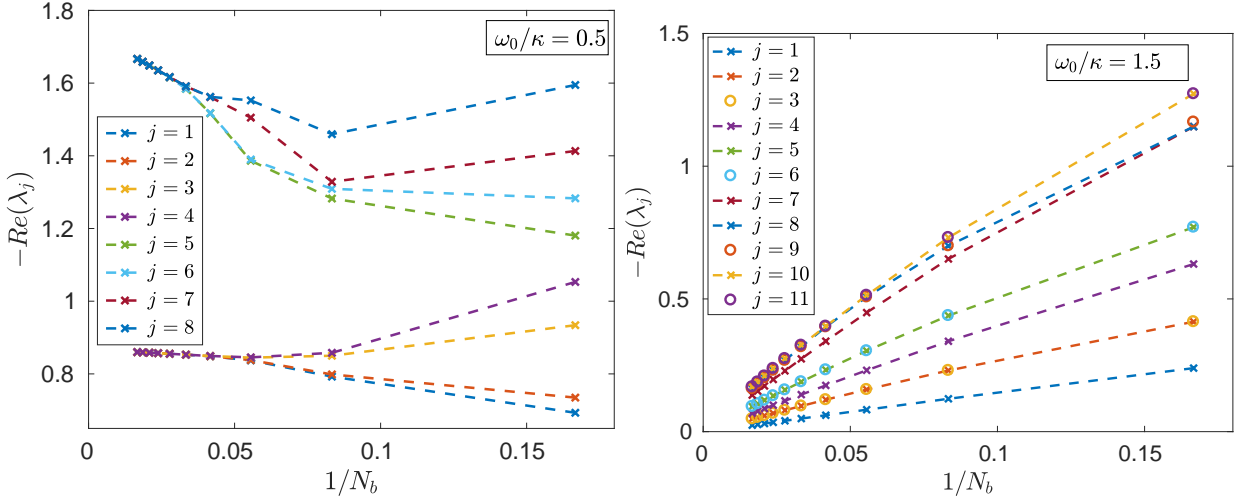


Figure S3. Finite size scaling for the real part of the Liouvillian eigenvalues in the two distinct phases of the model. (Left panel) For $\omega_0/\kappa = 0.5$ the gap in the Liouvillian spectrum persist in the thermodynamic limit $N_b \rightarrow \infty$ while for $\omega_0/\kappa = 1.5$ (right panel) the eigenvalues vanish algebraically with N_b .

In order to underline the connection of the spectral properties with the time-translation symmetry breaking oscillations, in Fig. S4 we plot the absolute value of the lowest excitation Liouvillian eigenvalue with nonvanishing imaginary part, $\lambda_{<}^{Im}$. Remarkably, this value provides a good approximation to the fundamental frequency of the band structure: $\lambda_{<}^{Im}/\Gamma_{\omega_0/\kappa} \sim 0.971$ (0.995) for $\omega_0/\kappa = 1.5$ (2) (see right panel of Fig. 3 of the main text). The fundamental frequency is here defined as the difference between the average position of two nearest bands. It also coincides with the frequency of the main peak in the Fourier transform of the oscillating time-translation symmetry breaking magnetization (see Fig. 4 of the main text).

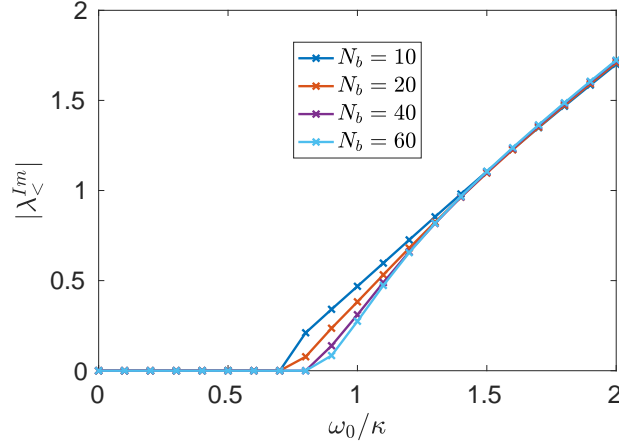


Figure S4. Lowest excitation eigenvalue of the Liouvillian with nonzero imaginary value.

SEMICLASSICAL LIMIT

Using the cyclic property of the trace, we can write the derivative of the expectation of any operator \hat{O} in the form

$$\begin{aligned} \frac{d}{dt} \langle \hat{O} \rangle &= \frac{d}{dt} \text{Tr}(\hat{O}\hat{\rho}) \\ &= i \text{Tr}([\hat{H}_b, \hat{O}]\hat{\rho}) + \frac{\kappa}{2S} \text{Tr}([\hat{S}_+, \hat{O}]\hat{S}_- + \hat{S}_+[\hat{O}, \hat{S}_-])\hat{\rho}. \end{aligned} \quad (\text{S11})$$

Taking for \hat{O} the three spin components and using the commutation relations $[\hat{S}^\alpha, \hat{S}^\beta] = i\epsilon^{\alpha\beta\gamma}\hat{S}^\gamma$, we find

$$\begin{aligned} \frac{d}{dt} \langle \hat{S}^x \rangle &= -\frac{\omega_z}{S} (\langle \hat{S}^y \hat{S}^z \rangle + \langle \hat{S}^z \hat{S}^y \rangle) + \frac{\kappa}{2S} (\langle \hat{S}^x \hat{S}^z \rangle + \langle \hat{S}^z \hat{S}^x \rangle + \langle \hat{S}^x \rangle) \\ \frac{d}{dt} \langle \hat{S}^y \rangle &= -\omega_0 \langle \hat{S}^z \rangle + \frac{(\omega_z - \omega_x)}{S} (\langle \hat{S}^x \hat{S}^z \rangle + \langle \hat{S}^z \hat{S}^x \rangle) + \frac{\kappa}{2S} (\langle \hat{S}^y \hat{S}^z \rangle + \langle \hat{S}^z \hat{S}^y \rangle - \langle \hat{S}^y \rangle) \\ \frac{d}{dt} \langle \hat{S}^z \rangle &= \omega_0 \langle \hat{S}^y \rangle - \frac{\kappa}{S} (\langle (\hat{S}^x)^2 \rangle + \langle (\hat{S}^y)^2 \rangle + \langle \hat{S}^z \rangle) + \frac{\omega_x}{S} (\langle \hat{S}^x \hat{S}^y \rangle + \langle \hat{S}^y \hat{S}^x \rangle). \end{aligned} \quad (\text{S12})$$

On approaching the thermodynamic limit $S \rightarrow \infty$ it is convenient to define the reduced operators $\hat{m}^\alpha = \hat{S}^\alpha/S$. From the spin commutation relations we easily see that $[\hat{m}^\alpha, \hat{m}^\beta] = i\epsilon^{\alpha\beta\gamma}\hat{m}^\gamma/S$: in the limit $S \rightarrow \infty$ these operators commute, therefore $\langle \hat{m}^z \hat{m}^x \rangle \simeq \langle \hat{m}^z \rangle \langle \hat{m}^x \rangle$. We can therefore write Eqs. (S12) as

$$\begin{aligned} \frac{d}{dt} m^x &= -2\omega_z m^y m^z + \kappa m^x m^z \\ \frac{d}{dt} m^y &= 2(\omega_z - \omega_x) m^x m^z - \omega_0 m^z + \kappa m^y m^z \\ \frac{d}{dt} m^z &= \omega_0 m^y - \kappa ((m^x)^2 + (m^y)^2) + 2\omega_x m^x m^y. \end{aligned} \quad (\text{S13})$$

up to corrections of order $1/S$. These equations conserve the norm $\mathcal{N} \equiv (m^x)^2 + (m^y)^2 + (m^z)^2$. When $\omega_z = \omega_x = 0$ there is another conserved quantity

$$\mathcal{M} \equiv \frac{m^x}{m^y - \omega_0/\kappa}. \quad (\text{S14})$$

It is easy to see that this quantity is conserved by comparing the first two equations of Eq. (S13), where we find $\frac{d}{dt} \log m^x = \frac{d}{dt} \log (m^y - \frac{\omega_0}{\kappa})$. Also for $\omega_z, \omega_x \neq 0$ it is possible to show that there is another conserved quantity beyond the norm. Let us consider first, for simplicity, the case in which $\omega_x = 0$. We can see that there is a conserved quantity which generalizes the one Eq. (S14) and has the form

$$\begin{aligned} \mathcal{R}_{\omega_z} &= 2\omega_z \log ((\kappa m^y + 2\omega_z m^x - \omega_0)^2 + (\kappa m^x - 2\omega_z m^y)^2) \\ &+ 2\kappa \text{atan} \left(\frac{\kappa m^x - 2\omega_z m^y}{\kappa m^y + 2\omega_z m^x - \omega_0} \right) + 2\kappa \pi n \end{aligned} \quad (\text{S15})$$

(details on the derivation of \mathcal{R}_{ω_z} are given in the section below). As the expression of the conserved quantity involves the arctangent, one may notice that this conserved quantity has multiple branches. i.e. the quantity is defined only up to integer multiples of $2\kappa\pi$. This means that on crossing the branch cut, $\kappa m^y + 2\omega_z m^x - \omega_0 = 0$, the conserved quantity can switch branch (add or subtract a multiple of $2\pi\kappa$). As a result, the conservation of \mathcal{R}_{ω_z} is consistent with a converging spiral toward the fixed point. When $\omega_z = 0$, \mathcal{R}_{ω_z} reduces to $\mathcal{R}_0 = 2\kappa \text{atan}(\mathcal{M})$, consistently with our previous finding. Therefore, whichever the parameters of the system, there exist two conserved quantities, \mathcal{N} and \mathcal{R}_{ω_z} . This property motivates the fact that this system never shows a single periodic attractor but can show closed periodic orbits in some regimes (in other regimes the attractor can be a fixed point, as demonstrated in Ref. [7] for $\frac{\omega_0}{\kappa} < 1$ and $\omega_z = 0$). A case in which the system can only show closed periodic orbits is $\omega_z = 0$ and $\frac{\omega_0}{\kappa} > 1$, the weak dissipation regime we extensively consider in the main text. We can see this fact in the phase space portrait in the upper-left panel of Fig. S5. For the phase space portraits we consider the coordinates \mathcal{Q} and \mathcal{P} defined as

$$\begin{aligned} \mathcal{Q} &= m^z \\ m^x &= \sqrt{1 - \mathcal{Q}^2} \cos(2\mathcal{P}) \\ m^y &= \sqrt{1 - \mathcal{Q}^2} \sin(2\mathcal{P}). \end{aligned} \tag{S16}$$

In the other panels we show the phase space portraits for different parameters. In the upper right panel we consider $\omega_0/\kappa > 1$ and ω_z small; we see that the dynamics is constrained over closed periodic orbits also in this case. Consistently with the existence of the conserved quantity Eq. (S15), the time-translation symmetry breaking is a phenomenon robust to this kind of perturbation of the Hamiltonian.

On increasing ω_z there is a transition to a different regime where in half of the phase space there are closed orbits, and in the other half there is a single-point attractor (lower panel of Fig. S5). We can understand this fact from an analytical point of view, looking for the fixed points of Eq. (S13). Imposing the time-derivatives equal to 0, and $\mathcal{N} = 1$, we find four fixed points: the trivial pair ($m^z = 0, m^y = \kappa/\omega_0, m^x = \pm\sqrt{1 - (\kappa/\omega_0)^2}$), and two non-trivial ones at

$$\begin{aligned} m^x &= \frac{2\omega_z\omega_0}{\sqrt{\kappa^2 + 4\omega_z^2}} \\ m^y &= \frac{\kappa\omega_0}{\sqrt{\kappa^2 + 4\omega_z^2}} \\ m^z &= \pm\sqrt{1 - \frac{\omega_0^2}{\sqrt{\kappa^2 + 4\omega_z^2}}}. \end{aligned} \tag{S17}$$

In order to find the non-trivial fixed points, we have to impose the argument of the square-root larger than 0, which gives the condition $\sqrt{\kappa^2 + \omega_z^2} \geq \omega_0$. With the parameters used in Fig. S5, the transition point is at $\omega_z = \frac{\sqrt{3}}{4}$, which agrees with the numerical observations. As we can see in the lower panels of Fig. S5, one of the two fixed points is attractive (the one on the left) and the other is repelling (the one on the right).

In the case where $\omega_x \neq 0$ it is also possible to derive a conserved quantity for the dynamics similar to Eq.(S15) (see the details for its derivation in Section below). In Fig.(S7) we show the phase space portrait for the dynamics of the system, where we see that the dynamics is also constrained over closed periodic orbits, corroborating our expectations on the stability of the time crystal phase.

It is worth noticing that the peculiar dynamics studied in this article belongs to the class of reversible systems [11], i.e., dynamical systems whose phase space variable “ x ” is invariant under the combination $t \rightarrow -t, x \rightarrow Gx$, with G representing an involution transformation ($G \circ G = \text{Identity}$). From our equations of motion (Eq. (S13)), we promptly identify the involution in our model as the transformation $m_x \rightarrow m_x, m_y \rightarrow m_y$ and $m_z \rightarrow -m_z$.

DERIVATION OF CONSERVED QUANTITIES $\mathcal{R}_{\omega_z, \omega_x}$

In order to construct a conserved quantity for ω_z and $\omega_x \neq 0$, with $\omega_z > \omega_x$, we rewrite the first two lines of Eq. (S13) as

$$\frac{1}{m^z} \frac{d}{dt} \begin{pmatrix} m^x \\ m^y \end{pmatrix} = \hat{A} \begin{pmatrix} m^x \\ m^y \end{pmatrix} + \begin{pmatrix} 0 \\ -\omega_0 \end{pmatrix}. \tag{S18}$$

with

$$\hat{A} = \begin{pmatrix} \kappa & -2\omega_z \\ 2(\omega_z - \omega_x) & \kappa \end{pmatrix} \quad (\text{S19})$$

Diagonalizing the \hat{A} matrix we obtain its eigenvalues and eigenvectors, given respectively by,

$$\lambda_{\pm} = \kappa \pm 2i\sqrt{\omega_z(\omega_z - \omega_x)}, \quad \hat{u}_{\pm} = \frac{1}{\sqrt{c}} \begin{pmatrix} 1 \\ \mp i\sqrt{1 - \omega_x/\omega_z} \end{pmatrix} \quad (\text{S20})$$

with $c = 2 - \omega_x/\omega_z$ the normalization constant. We can now rewrite Eq.(S18) in this eigenbasis, obtaining

$$\frac{d}{dt}\hat{\eta}_{\pm} = \left(\lambda_{\pm}\hat{\eta}_{\pm} - \frac{\omega_0}{\sqrt{c}} \right) m^z \quad (\text{S21})$$

where $\hat{\eta}_{\pm} = \hat{u}_{\pm} \cdot (m_x, m_y)^T$. In other words, we have that,

$$\frac{1}{\lambda_{\pm}} \frac{d}{dt} \log \left(\lambda_{\pm}\hat{\eta}_{\pm} - \frac{\omega_0}{\sqrt{c}} \right) = m^z \quad (\text{S22})$$

From this last relation we directly find the conserved quantity,

$$\mathcal{R}_{\omega_z, \omega_x} \equiv -i \left[\lambda_- \log \left(\lambda_+ \hat{\eta}_+ - \frac{\omega_0}{\sqrt{c}} \right) - \lambda_+ \log \left(\lambda_- \hat{\eta}_- - \frac{\omega_0}{\sqrt{c}} \right) \right] \quad (\text{S23})$$

which is clearly real being $\lambda_+ = \lambda_-^*$. Considering, for example, the case with $\omega_x = 0$, we can expand the terms in the conserved quantity as,

$$\mathcal{R}_{\omega_z} = (-i\kappa + 2\omega_z) \log \left(im^x + m^y - \frac{\omega_0}{(\kappa - 2i\omega_z)} \right) - (-i\kappa - 2\omega_z) \log \left(-im^x + m^y - \frac{\omega_0}{(\kappa + 2i\omega_z)} \right). \quad (\text{S24})$$

in which after some straightforward formal manipulations we get Eq. (S15), up to an immaterial constant which we do neglect. Due to the branch cut of the logarithms, the quantity in Eq. (S15) is defined only up to integer multiples of $2\kappa\pi$. This offset is determined by the number of times the branch cut is crossed. We show an instance of this fact in Fig. S6, where we consider the case of trajectories spiraling towards the attracting fixed point. The solid blue line marks the branch cut, the red lines mark different trajectories with different values of \mathcal{R}_{ω_z} : each time a trajectory crosses the branch cut, the value of \mathcal{R}_{ω_z} increases by $2\pi\kappa$.

-
- [1] Javier Prior, Alex W. Chin, Susana F. Huelga and Martin B. Plenio, Phys. Rev. Lett. **105**, 050404 (2010).
 - [2] Robert Rosenbach, Javier Cerrillo, Susana F. Huelga, Jianshu Cao and Martin B. Plenio, New. J. Phys. **18**, 023035 (2016).
 - [3] D. F. Walls, P. D. Drummond, S. S. Hassan, and H. J. Carmichael, Prog. Theo. Phys. **64**, 307 (1978).
 - [4] P. D. Drummond and H. J. Carmichael, Opt. Commun. **27**, 160 (1978).
 - [5] D. F. Walls, J. Phys. B: Atom. Molec. Phys. **13**, 2001-2009 (1980).
 - [6] S. Schneider and G. J. Milburn, Phys. Rev. A **65**, 042107 (2002).
 - [7] J. Hannukainen and J. Larson, arXiv:1703.10238.
 - [8] H. A. Sambe, Phys. Rev. A **7**, 2203 (1973).
 - [9] T. E. Lee, H. Häffner, and M. C. Cross, Phys. Rev. A **84**, 416, 031402 (2011).
 - [10] C.-K. Chan, T. E. Lee, and S. Gopalakrishnan, Phys. Rev. A **91**, 051601 (2015).
 - [11] J.A.G.Roberts and G. R. W. Quispel, **216**, 63-177 (1992).

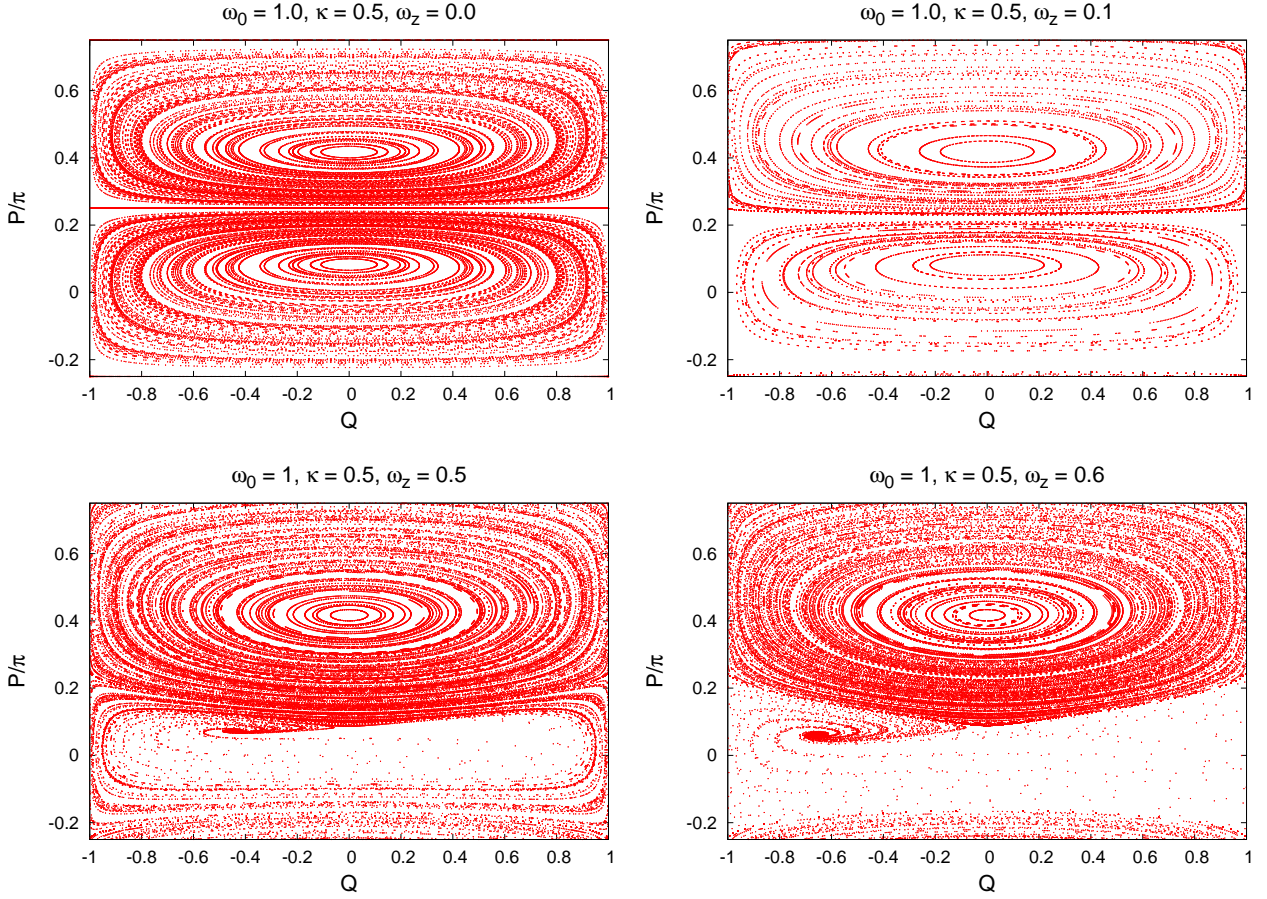


Figure S5. Phase space portraits for the dynamics in Eqs. (S13), with $\omega_x = 0$, for different values of the system parameters. We see that for small values of ω_z the dynamics is constrained to closed periodic orbits, while for larger values there is a portion of phase space where initial conditions are attracted towards a stable fixed point.

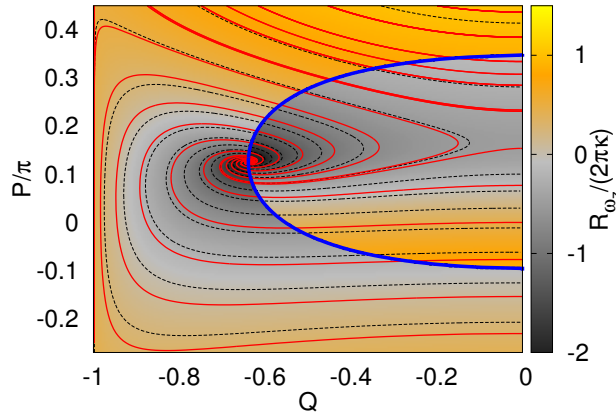


Figure S6. Trajectories (red solid) spiraling towards the fixed point and the branch cut of the difference of the logarithms in Eq. (S24) (blue solid line). The color-scale and gray-dashed contours correspond to the conserved quantity $\mathcal{R}/2\pi\kappa$ (Numerical parameters: $\omega_0/\kappa = 2.0$, $\omega_z/\kappa = 1.2$).

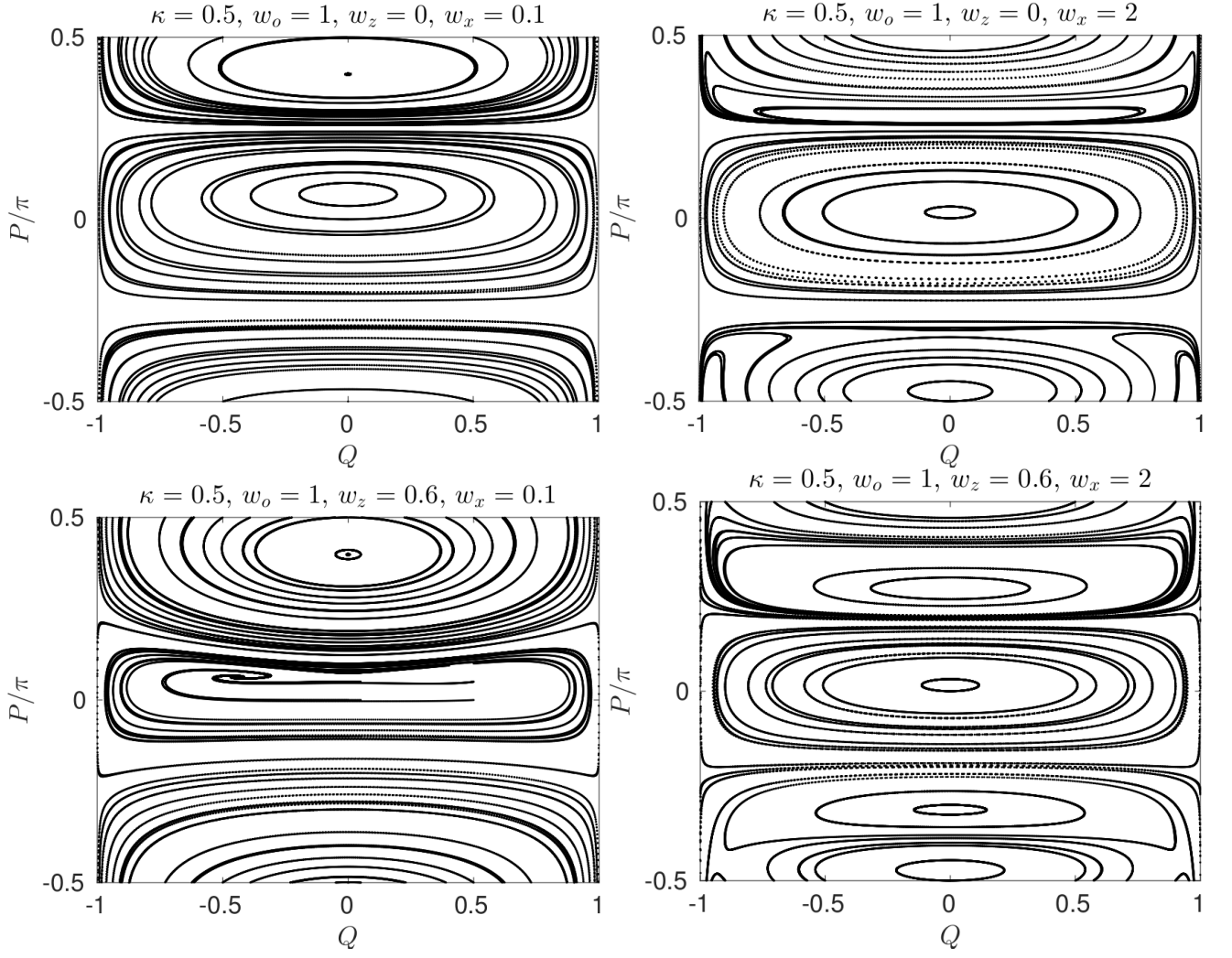


Figure S7. Phase space portraits for the dynamics in Eqs. (S13), with $\omega_x \neq 0$, for different values of the system parameters. We see that even for large values of ω_x the dynamics is still constrained to closed periodic orbits. In fact, such term improves the stability of the time crystal: the attractive fixed point in the lower left-panel stabilizes to periodic orbits (lower right-panel) at larger values of ω_x .